Original Research Article: Enhance and Performance Evolution of Silver-Doped Titanium Dioxide Dye-Sensitized Solar Cells Using Different Dyes

Sandra Onyeka Malumi[1], Temitope Malumi[2], Mike Onyehachukwu Osiele[3], Arthur Ekpekpo[3], Imosobomeh Lucky Ikhioya [4, 5]*

[1] *Department of Physics, Delta State University of Science and Technology, Ozoro, Delta State, Nigeria*
[2] *School of Organizations, Systems, and People, University of Portsmouth, England, United Kingdom*
[3] *Department of Physics, Delta State University, Abraka, Delta State, Nigeria*
[4] *Department of Physics and Astronomy, University of Nigeria, Nsukka, 410001, Enugu State, Nigeria*
[5] *National Centre for Physics, Quaid-i-Azam University Campus, Islamabad, 44000, Pakistan*

Use yor device to scan and read the article online

Citation S. O. Malumi, T. Malumi, M. O. Osiele, A. Ekpekpo, I.L. Ikhioya*. Enhance and Performance Evolution of Silver-Doped Titanium Dioxide Dye-Sensitized Solar Cells Using Different Dyes. *J. Eng. Ind. Res.* **2023**, 4 (4):189-200.

https://doi.org/10.48309/JEIRES.2023.4.1

Article info:
Received: 2023-10-26
Accepted: 2023-12-23
ID: JEIRES-2311-1106
Checked for Plagiarism: Yes
Editor who Approved Publication:
Professor Dr. Mohammad Haghighi

Keywords:
Titanium dioxide; Efficiency; DSSCs; FTO; Dye.

ABSTRACT

In this study, silver was used to doped TiO_2 with *Azadirachtaindica*(neem), *Annonamuricata* (Soursop leaf), *Manihotesculenta* (cassava leaf), and Myrianthusarboreus (Coat button leaf) for DSSCs fabrication. The sensitized TiO_2/silver with dye recorded an efficiency of 0.49%, 0.03%, 0.05%, and 0.22% for *Azadirachtaindica* (neem), *Annonamuricata* (Soursop leaf), *Manihotesculenta* (cassava leaf), and Myrianthusarboreus (giant yellow mullbery leaf), respectively. The optical energy bandgap was observed to be 2.32 eV for TiO_2 and 2.52 eV, 2.31 eV, 2.49 eV, and 2.51 eV for Neem, Soursop Cassava, and Giant yellow mullbery leaf dye. The structure of the cells is polycrystalline with a most outstanding peak at 2 theta angles of 30.375° and 30.464° corresponding to (200). Therefore, the secondary peaks were noticed at 2 theta angles of 24.891°, 27.509°, 32.915°, 27.509°, 35.296°, 38.814°, 43.152°, 47.579°, 53.231°, and 59.130° for TiO_2.

Introduction

Dye-sensitized solar cells belong to the family of photo-electrochemical cells. DSSs stand out from other solar cells because they separate charges [1]. DSSCs offer green energy capabilities, affordability, and easy production. DSSCs are efficient for indoor lighting and electronic applications, like wireless sensors [2]. The abundance of materials, reasonable cost, and lightweight, flexible, and thin solar modules

***Corresponding Author: Imosobomeh L. Ikhioya** (imosobomeh.ikhioya@unn.edu.ng)*

emphasize the potential of their affordable interior photovoltaics. Scaling up fabrication techniques is necessary for achieving performance stability and photovoltaic efficiency in indoor environments [3]. The DSSCS uses two glass electrodes, with a metal oxide film coated in dye-adsorbed zinc oxide and titanium dioxide nanoparticles. The DSSCS uses a graphite or platinum-coated counter electrode, while the electrolyte solution containing the redox couple refreshes the dye. Nanostructured metal oxide coatings are attractive for DSSCs because of their large surface area [4]. The wide band gap energy, high conduction band edge, large surface area, and excellent chemical stability of TiO_2 make it the semiconductor of choice in DSSC structures [5].Various metal oxide semiconductors, including Nb_2O_5, SnO_2, and ZnO, have been used as electron transport layers in DSSCs, with ZnO exhibiting the highest electron transport capability. Although ZnO-based DSSCs are less efficient than TiO_2-based devices, the inexpensive and straightforward synthesis methods of ZnO make it an attractive alternative [6]. It can be produced in different forms, like nanowires, nanotubes, and nanotips. The combination of ZnO and TiO_2 has been studied using various methods, including adding ZnO powder to TiO_2 or mixing both oxides during synthesis [7-9]. These procedures can cause a structure comprising a blend of ZnO and TiO_2 nanoparticles or core–shell structure [10-12]. Different techniques were employed to merge ZnO nanoflowers with TiO_2.

Despite having the largest economy in Sub-Saharan Africa, Nigeria's progress is hindered by electricity shortages. Nigeria possesses ample oil, gas, hydro, and solar resources, with current infrastructure capable of generating 12,522 MW of electricity. It can only generate around 4,000 MW on most days, which falls short for a country with a population of over 195 million people. In 2011, Nigeria's primary energy consumption reached approximately 108 Mtoe. Biomass and garbage handle 83% of total primary production, serving as the major energy sources. Fossil fuels account for 16%, while hydropower contributes 1% [13-16]. The concept of harnessing solar energy has captivated scientists, leading to extensive research on understanding and imitating photosynthesis. In 1912, a proposal was made to replace fossil fuels with solar electricity radiation from the Sun after extensive research. Greenhouse gases like carbon dioxide and methane are produced through the combustion of fossil fuels, leading to pollution, global warming, and climatic shifts. With fossil fuels depleting and petrol and diesel prices rising, we need alternate renewable energy sources [17]-[21]. To avert this disaster, research is being done to substitute fossil fuels with solar energy.

The sun radiates heat and light, known as solar energy. It is the boundless energy source of the world. The sun's energy, up to 100,000 terawatts (TW), transforms into various other forms after being reflected and absorbed in the atmosphere. The Chemical American Society's 2010 chemical review journal calculated that the sun provides 6,000 times the global primary energy [6,10,12,22].Global consumption increased to 28TW in 2015 due to population growth. Our global energy demand requires a substantial amount of low energy. The DSSC working concept resembles the photosynthesis response of green plants. Chemical energy is produced from light during photosynthesis. Electrons are ejected when photons hit chlorophyll and other pigments due to photo-induced charge separation. Light absorption by a photoactive molecule is essential for the operation of photovoltaic cells in DSSC. A DSSC operates by sensitizing a metal oxide semiconductor, like TiO_2 or ZnO (n-type) and NiO (p-type), with a monolayer of a molecular dye attached to its surface [23-27]. The dye soaks up light within the visible spectrum (400-700nm).The dye is crucial for assembling a DSSC.

The numerous advantages of titanium dioxide made it the preferred semiconductor for the photoelectrode.It's inexpensive, easily accessible, and safe.Sensitizers like [Ru(4,40 -dicarboxylic-2, 20-bipyridine ligand)3] were used early on and remain the most commonly employed. Typically, the main redox couple used is triiodide/iodine [24-29].Optimization and compatibility of the constituents, especially the semiconductor film and dye spectral responses, play a crucial role in determining the total

efficiency of the dye-sensitized solar cell. The high surface area of the semiconductor film is a crucial factor that leads to increased dye loading and optical density, enabling efficient light harvesting. Doping transition metal ions can enhance TiO_2's photocatalytic efficiency, but the material's activity also relies on the preparation method and catalyst properties. Various TiO_2 synthesis methods, such as sol-gel, have been proposed in the literature. The sol-gel process is a highly desirable way to incorporate foreign metal ions into TiO_2 powders and films. Metal ions like iron, copper, and cobalt have been used as acceptor dopants in TiO_2, resulting in improved photocatalytic activity to different degrees [30-35]. In this study, silver was used to doped TiO_2 with *Azadirachtaindica*(neem), *Annonamuricata* (Soursop leaf), *Manihotesculenta* (cassava leaf), and Myrianthus arboreous (Coat button leaf) for DSSCs fabrication.

Experimental procedure

Materials

Materials used in this research are 100 ml and 200 ml glass beakers, glass rod, masking tape, ceramic mortar and pestle, model: HK-DC-320AS weighing scale, aluminum foil, syringes, filter papers, distilled water, liquid iodide redox electrolyte, crocodile clips, Rheostat, negative and positive terminal probes (wire), glass slides, diamond cutter, magnetic stirrer, Electric Heated Blast dry Box (Oven SM-9023), Ultrasonic machine, thermostatic oven of 50 ˚C-1000 ˚C, ohmmeter, Fluorine doped tin oxide (FTO) glass, 3 g of Titanium Oxide (TiO_2) powder, Silver nitrate ($AgNO_3$), Acetone, Methanol and the leaves used *tridaxpnocumbens* (giant yellow mullbery*)*, *azadirachtaindica (neem leaf)*, *annonamuricata (soursop leaf)*, *manihotesculenta (cassava leaf)*. These materials were used besides the usual equipment for characterization.

Natural dye extraction

The fresh leaves of *tridaxpnocumbens (*giant yellow mullbery*)*, *azadirachtaindica (neem leaf)*, *annonamuricata (soursop leaf)*, and *manihotesculenta (cassava leaf)* were harvested and bought from different local farms within Delta State. The leaves were rinsed thoroughly with distilled water and air dried until they became invariant for two weeks at a room temperature range of 24 °C-32 °C. The leaves were grinded using an electric blender to form a powder. 50 g of each ground leaf is measured using a weighing scale and put in a 500 ml beaker, and then soaked with 100 ml of methanol and stirred on a magnetic stirrer for 3hours. Thereafter, the mixture was covered with an aluminum foil sheet and set aside for 24hours, as displayed in Figure 1. The dyes from the leaves were then extracted into a beaker with the help of filter paper. The samples are poured into containers and stored away from sunlight. The purpose was to avoid dyes deterioration.

Preparation of substrate (FTO glass)

To dissolve the unwanted organic materials and remove any dust and contamination left on the substrate after manufacturing, the FTO glass was cleaned by immersing it successively in acetone and distilled water for approximately 30 minutes each in an ultrasonic bath before cell fabrication. The process continues with an additional 20 minutes of ultrasonic bath using methanol to eliminate the residual acetone and other impurities. The substrate was heated to 50 °C using a hot air oven for deposition.

Preparation of the Photoanode Deposition on FTO glass

To prepare the TiO_2 thin film electrode (photoanode), the Doctor Blade technique was employed. The term "Doctor Blade" refers to a film smoothing technique involving the use of a steel, rubber, plastic, or similar blade to apply or remove a liquid substance from a surface [10]. By adding 5 ml of methanol to 3 g of TiO_2 powder drop by drop in a mortar while grinding and stirring with a pestle, the TiO_2 paste was prepared, and aggregated particles of TiO2 were mechanically separated. During the process of the cell fabrication, 0.1 mol silver nitrate ($AgNO_3$) was used to dope the TiO_2, and the silver nitrate ($AgNO_3$) was dissolved with 2 ml of

methanol before adding to the TiO_2 paste. A substrate made of transparent fluorine-doped tin oxide (FTO) conducting glass, measuring on average 2.25 cm by 2.35 cm, was used for the deposition of TiO2/silver nitrate ($AgNO_3$) paste. An ohmmeter was used to check for the conductive side of the glass. Two transparent FTO conducting glasses were used during the deposition. While one is the depositing surface, the other is used as a guide to ensure uniformity. Paper tape was applied on the conductive side to mask 0.15-0.2 cm at the three edges of the depositing glass surface and the opposite sides of the guiding slide in Figure 2. A glass rod is used to ensure that there is no opening into the masked edges. The TiO_2 colloidal solution was evenly applied to the substrate using drops, and then uniformly spread using a glass stirring rod. Annealing the grown films was performed at 250 °C for 30 minutes using an oven with a temperature range of 50 °C-1000 °C, and then it was cooled and prepared for sensitization.

Dye loading

TiO_2/Silver nitrate-coated glass films were sensitized separately in various dye extracts presented in Table 1 for approximately 24 hours (Figure 3).The stained film of TiO_2/silver nitrate ($AgNO_3$) is eliminated by using a thong. Then, the sample is positioned on a rack with the stained side facing upwards.

Figure 1: The dye extract later covered with an aluminum sheet.

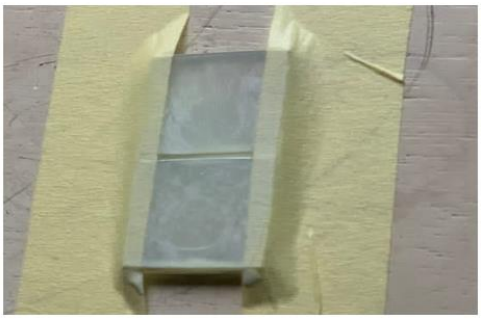

Figure 2: The photoanode deposition on the FTO glass. **Figure 3:** The dye-coated photoanode layers.

Table 1: Loaded dyes on the coated glass film and the dye combination

FTO Coated glass films. Titled	Molecular concentration (mol)	Doped TiO_2photoanode	Dye solution present
1	0.1	TiO_2 /silver nitrate	20ml Neem dye
2	0.1	TiO_2 /silver nitrate	20ml Soursop dye
3	0.1	TiO_2 /silver nitrate	20ml Cassava dye
4	0.1	TiO_2 /silver nitrate	20ml Coat button dye

Preparation of counter electrode

The counter electrode was fabricated from an alternative conductive glass. The glass was checked for conductivity using an ohmmeter. The conductive side of the glass substrate in Figure 4 is coated using a carbon pencil. The electrode did not need any masking or tape, so the entire surface was coated to increase its area. The redox electrolyte used was the KI/Iodine electrolyte solution from the Institute of Chemical Education (ICE).

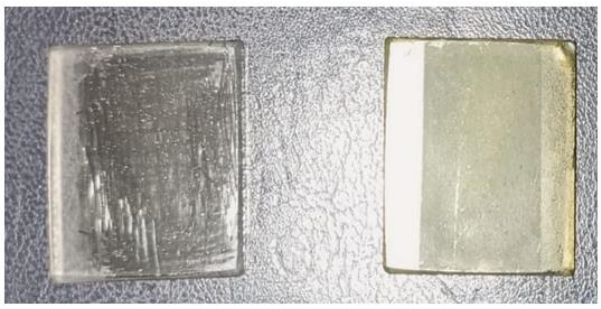

Figure 4: The conductive side of the counter electrode coated with a pencil carbon.

Assembly of DSSC and electrical output measurement

The TiO_2/silver nitrate ($AgNO_3$) electrode with dye was positioned on the lab table, film side up. The counter electrode was then placed on top, ensuring direct contact with the conductive side of the TiO_2/silver nitrate ($AgNO_3$) electrode. The two glass slides were positioned that covered all TiO_2/silver nitrate ($AgNO_3$) with the counter electrode, leaving only the 0.2 cm strip of uncoated glass exposed.

Two crocodile clips were used to secure the slides together at the other edges in Figure 5.The slides were injected with a solution of potassium iodide-iodine (KI/Iodine) electrolyte through the edges. The finished solar cell was measured to determine its current-voltage characteristics

Figure 5: The fabricated solar cell and DSSC undergoing electrical testing by the use of a digital source meter.

Results

Optical Study of TiO2 and TiO2 /Ag0.1/dyes

The optical analysis of the silver-doped TiO_2 and dye-sanitized material is shown in Figure 6a. The absorbance decreases with the increase in the wavelength of electromagnetic radiation. The dye-sensitized material has a reduction up to 610 nm and a prominent peak from 650 to 702 nm. The peak that stands out, shows that silver and dye are present. The dye-sensitized material experienced a peak at different wavelengths, namely 682, 619, 700, and 617 nm for giant yellow mullbery, Neem, Cassava, and Soursop leaf dye, respectively. From 703 to 1100 nm, the dye-sanitized material undergoes a decrease. By introducing silver as a dopant, the absorbance feature of the cells is enhanced. Fabricated cells are perfect for solar and other light-emitting applications. The analysis of transmittance for the silver-doped TiO_2 and dye-sensitized material is shown in Figure 6b. Electromagnetic radiation's wavelength increases, leading to an increase in transmittance.

The dye-sensitized material exhibits a peak increase of up to 610 nm with a significant peak ranging from 650 to 702 nm. The prominent peak shows silver and dye. The dye-sensitized material peaked at different wavelengths, i.e. 682, 619, 700, and 617 nm for giant yellow mullbery, Neem, Cassava, and Soursop leaf dye, respectively. There is an increase in the dye-sensitized material between 703 and 1100 nm. The silver addition as a dopant improves the transmittance characteristic of the cells.

Fabricated cells are ideal for use in solar and other light-emitting applications.

Figure 6c displays the reflectance analysis of the dye-sensitized material and silver-doped TiO_2. The reflectance increases as the wavelength of electromagnetic radiation increases. The dye-sensitized material shows a maximum surge of 610 nm with a considerable peak between 650 to 702 nm. Silver and dye are visible on the prominent peak. We observed different wavelengths for the dye-sensitized material, giant yellow mulberry, Neem, Cassava, and Soursop leaf dye have wavelengths of 682, 619, 700, and 617 nm, respectively. The dye-sensitized material has increased between 703 and 1100 nm. The silver addition as a dopant increases cell transmittance.

The material's transmittance changes with wavelength, showing that silver and dye improve the cell's photovoltaic properties. Fabricated cells are a great fit for solar and other light-emitting applications. The estimation of the energy bandgap of dye-sensitized material and silver-doped TiO_2 can be seen in Figure 6d, where the straight part of the Tauc plots is extrapolated. This can be accomplished because the absorption coefficient (α) can be stated as $\alpha h\nu=(h\nu - E_g)^{1/2}$, where Eg, hv, α, and A are the optical energy bandgap, photon energy, absorption coefficient, and constant, respectively, and the intercept on the horizontal axes gives a good estimation of the optical energy bandgap.

Based on the results, the optical energy bandgap was observed to be 2.32 eV for TiO_2 and 2.52 eV, 2.31 eV, 2.49 eV, 2.51 eV [15-16,34-36] for Neem, Soursop Cassava, and giant yellow mullbery leaf dye.

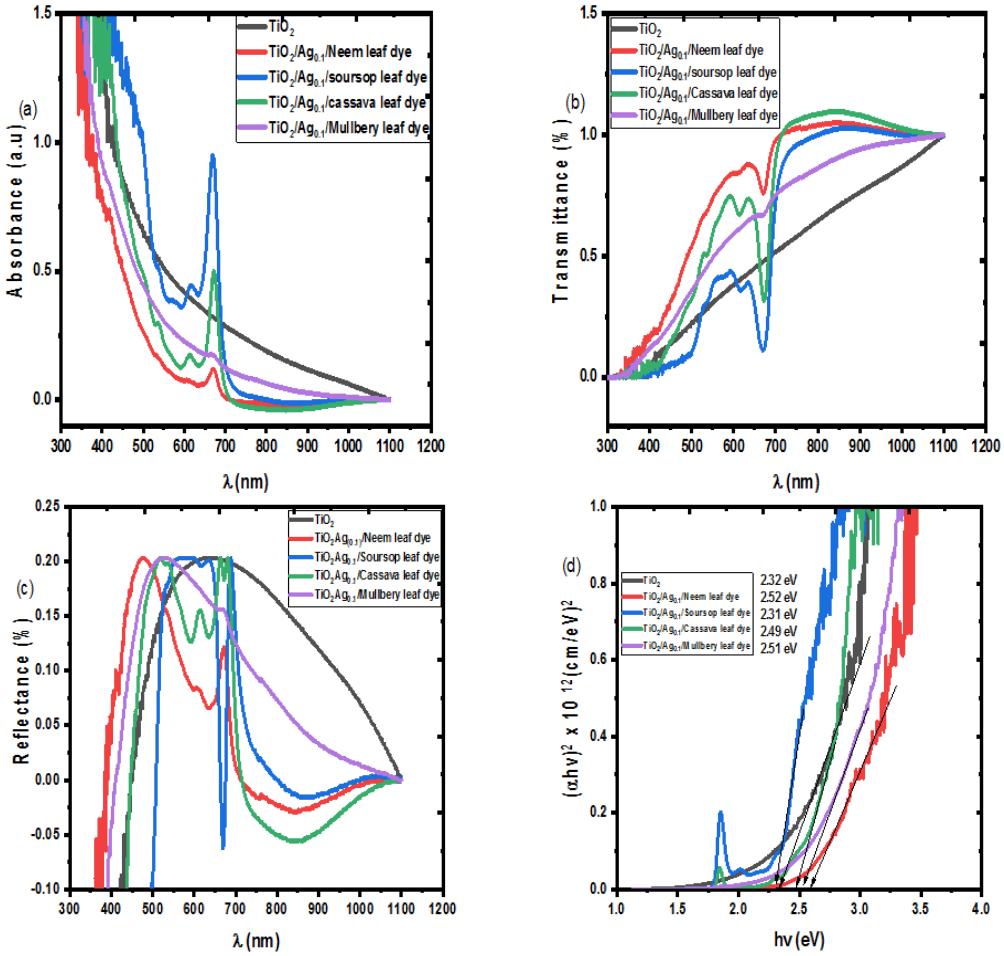

Figure 6: Absorb (a), Transmitt (b), Reflect (c), and Energy bandgap (d).

Table 2: The Photovoltaic performance of the TiO_2 mesoporous films sensitized by natural dye extract

Sensitized TiO_2 mesoporous films	V_{oc} (V)	I_{sc} (mA/cm²)	V_{max} (V)	I_{max} (mA/cm²)	P_{max} (mWcm^{-2})	Fill Factor	Efficiency η(%)
$TiO_2/Ag_{0.1}$/Neem dye	0.425	1.140	0.290	0.814	0.236	65.309	0.49
$TiO_2/Ag_{0.1}$/Soursop dye	0.392	0.627	0.241	0.423	0.102	35.995	0.03
$TiO_2/Ag_{0.1}$/Cassava dye	0.465	0.692	0.324	0.510	0.165	50.896	0.05
$TiO_2/Ag_{0.1}$/ giant yellow mullbery dye	0.474	1.075	0.320	0.798	0.255	43.817	0.22

Photovoltaic Results of the Fabricated DSSCs

The DSSC devices were tested under incident illumination of 880 mW/cm^2, using a cell area of 2.25 cm by 2.35 cm to determine their photovoltaic parameters. The J-V curves for the DSSC devices are illustrated in Figure 7, and Table 2 presents the gained J-V parameters. The DSSC contained natural dye extracts derived from Azadirachtaindica (neem) (a), Annonamuricata (Soursop leaf) (b), Manihotesculenta (cassava leaf) (c), and Myrianthusarboreus (Giant yellow mullbery leaf) (d) sources. The open-circuit voltage (Voc) remains consistent across all samples, indicating that natural dye extracts have a minimal effect on the DSSC's voltage potential. The sensitized TiO_2/silver with dye recorded the efficiency of 0.49%, 0.03%, 0.05%, and 0.22% [36] for *Azadirachtaindica*(neem), *Annonamuricata* (Soursop leaf), *Manihotesculenta* (cassava leaf), and Myrianthusarboreus (giant yellow mullbery leaf), respectively.

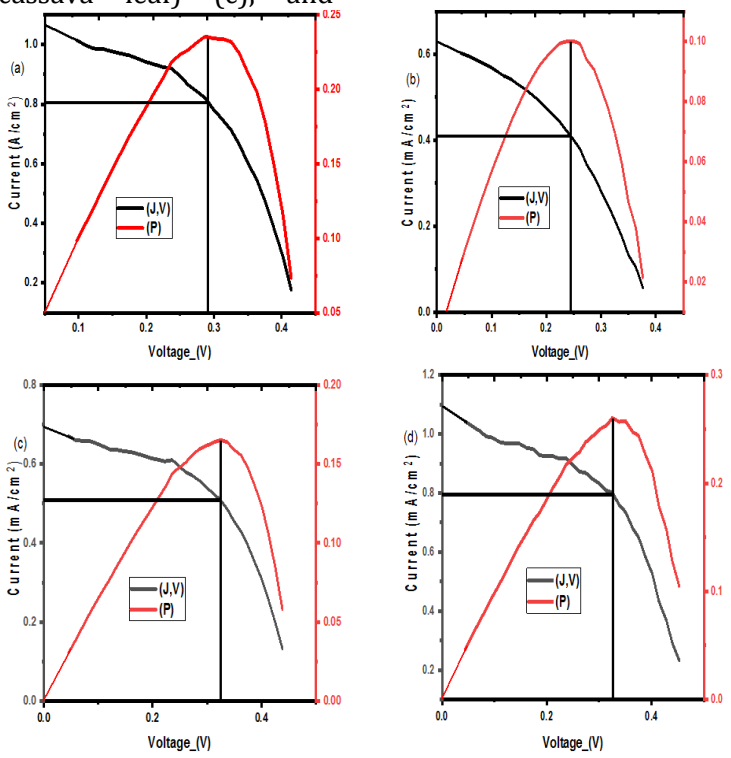

Figure 7: Light J-V curve of DSSC sensitized with the dye extract from *Azadirachtaindica*(neem) (a) *Annonamuricata* (Soursop leaf) (b), *Manihotesculenta* (cassava leaf) (c), and Myrianthus arboreous (Giant yellow mullbery leaf) (d)

SEM analysis of TiO2 and TiO2 /Ag0.1/dyes

Figure 8 demonstrates the surface morphology of the synthesized TiO_2 and $TiO_2/Ag_{0.1}$/dyes. The surface micrograph of TiO_2 reveals a nano growth of some clouded nanoparticles. The FTO substrate has a well-deposited TiO_2 synthesis on its surface. When the silver (Ag) and dye were deposited on top of the TiO_2, it completely changed the surface area. The synthesized material's surface changed from clouded nanoparticles to thinning nanoparticles, as seen in the film's micrograph of Neem leaf dye.

The surface micrograph of soursop leaf dye shows the adhesion of nanoflake particles on the substrate's surface. The micrograph displays nanorods of cassava leaf dye adhering tightly to the substrate [15-16,34-36]. The TiO_2, along with silver and dye, enhances the surface energy of the synthesized material for solar and photovoltaic applications. The EDX spectrum of the synthesized TiO_2 and TiO_2/Ag0.1/dyes is depicted in Figure 9. It is evident from the spectrum that all the elements composing TiO_2 are present.

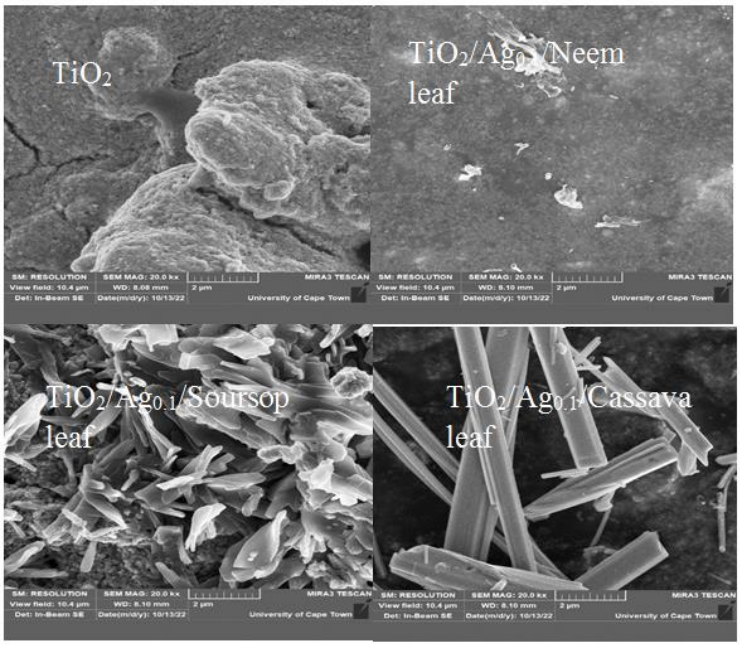

Figure 8: SEM of TiO_2 and TiO_2 /$Ag_{0.1}$/dyes

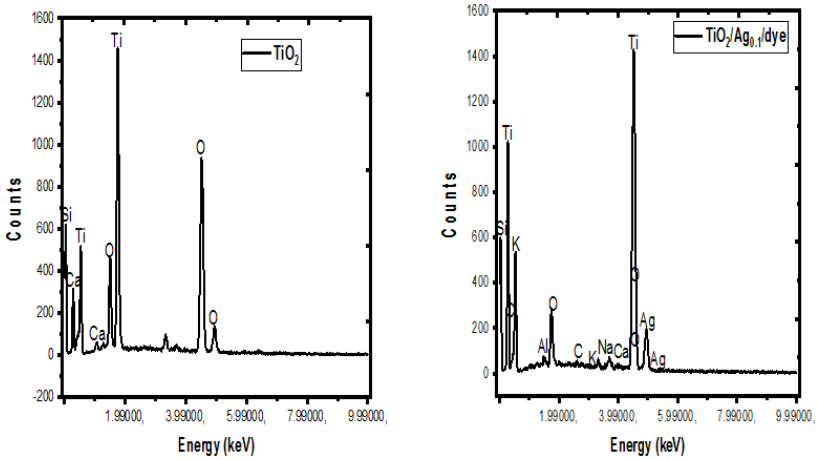

Figure 9: EDX spectrum of TiO_2 and TiO_2 /$Ag_{0.1}$/dyes

X-Ray Diffraction (XRD)

The XRD study of the synthesized TiO_2, $TiO_2/Ag_{0.1}$/Neem leaf, $TiO_2/Ag_{0.1}$/soursop leaf, and $TiO_2/Ag_{0.1}$/cassava leaf is illustrated in Figure 10.

The structure of the cells is polycrystalline with a most outstanding peak at 2 theta angles of 30.375 ° and 30.464 ° corresponding to (200). Therefore, the secondary peaks were noticed at 2 theta angles of 24.891°, 27.509°, 32.915°, 27.509°, 35.296°, 38.814°, 43.152°, 47.579°, 53.231° and 59.130 ° for TiO_2 and 26.116°, 27.835°, 32.667°, 36.195°, 39.802°, 41.926°, 47.173°, 52.084°, and 58.152° for $TiO_2/Ag_{0.1}$/Neem leaf, $TiO_2/Ag_{0.1}$/soursop leaf, and $TiO_2/Ag_{0.1}$/cassava leaf which corresponds to (101), (004), (105), (211), (204), (116), (220), and (215) and (303) subsequently [15-16,34-36]. The increase in peak intensity is because of the improved crystal structure and energy absorption on TiO_2's lattice parameters. The energy absorption of the crystals did not cause any shift in the peak locations. The shifts in the orientation of the crystals result from the dye causing the structure of the lattice and single-cell distortion. Equation (1) [30-35,37-40] was used to calculate the crystallite or grain size.

$$D = \frac{0.9\lambda}{\beta\cos\theta} \quad (1)$$

The grain size for TiO_2,$TiO_2/Ag_{0.1}$/Neem leaf, $TiO_2/Ag_{0.1}$/soursop leaf, and $TiO_2/Ag_{0.1}$/cassava leaf is indicated in Table 3. The films' crystallinity is improved by the increase in grain size.

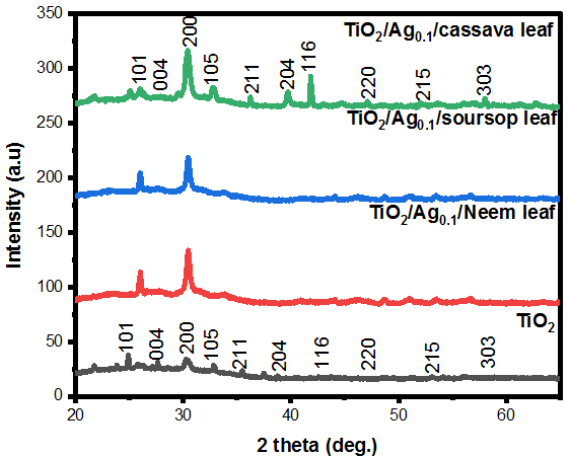

Figure 10: XRD pattern of TiO_2 and$TiO_2/Ag_{0.1}$/dy

Table 3: Structural variables for the synthesized films

Films	2θ (°)	d-spacing (Å)	FWHM	(hkl)	Lattice constant a (A)	Dislocation density (δ)	Grain Size (D) nm
TiO_2	24.891	3.573	0.109	101	6.190	1.795	1.302
	27.509	3.239	0.112	004	6.478	1.875	1.274
	30.375	2.939	0.113	200	5.879	1.884	1.271
	32.915	2.718	0.114	105	6.079	1.893	1.268
	35.296	2.540	0.117	211	6.222	1.969	1.243
	38.814	2.317	0.119	204	6.556	1.996	1.235
	43.152	2.094	0.120	116	5.924	1.973	1.242
	47.579	1.909	0.123	220	6.332	2.007	1.231
	53.231	1.719	0.127	215	5.955	2.042	1.221
	59.130	1.560	0.129	303	5.840	1.994	1.235

Table 3. Continued...

Films	2θ (°)	d-spacing (Å)	FWHM	(hkl)	Lattice constant a (A)	Dislocation density (δ)	Grain Size (D) nm
$TiO_2/Ag_{0.1}$/neem leaf	26.116	3.408	0.110	101	5.904	1.819	1.293
	27.835	3.202	0.111	004	6.404	1.839	1.286
	30.464	2.931	0.112	200	5.863	1.850	1.283
	32.667	2.738	0.113	105	6.123	1.863	1.278
	36.195	2.479	0.114	211	6.073	1.860	1.279
	39.802	2.262	0.116	204	6.399	1.885	1.271
	41.926	2.152	0.121	116	6.089	2.022	1.227
	47.173	1.924	0.122	220	6.384	1.980	1.240
	52.084	1.754	0.123	215	6.077	1.935	1.254
	58.152	1.584	0.123	303	5.930	1.831	1.289
$TiO_2/Ag_{0.1}$/soursop leaf	26.116	3.408	0.105	101	5.904	1.657	1.355
	27.835	3.202	0.113	004	6.404	1.906	1.264
	30.464	2.931	0.114	200	5.863	1.917	1.260
	32.667	2.738	0.115	105	6.123	1.929	1.256
	36.195	2.479	0.116	211	6.073	1.926	1.257
	39.802	2.262	0.117	204	6.399	1.917	1.260
	41.926	2.152	0.121	116	6.089	2.022	1.227
	47.173	1.924	0.122	220	6.384	1.980	1.240
	52.084	1.754	0.123	215	6.077	1.935	1.254
	58.152	1.584	0.125	303	5.930	1.891	1.269
$TiO_2/Ag_{0.1}$/cassava leaf	26.116	3.408	0.107	101	5.904	1.721	1.330
	27.835	3.202	0.111	004	6.404	1.839	1.286
	30.464	2.931	0.112	200	5.863	1.850	1.283
	32.667	2.738	0.113	105	6.123	1.863	1.278
	36.195	2.479	0.114	211	6.073	1.860	1.279
	39.802	2.262	0.115	204	6.399	1.852	1.282
	41.926	2.152	0.122	116	6.089	2.056	1.217
	47.173	1.924	0.123	220	6.384	2.013	1.230
	52.084	1.754	0.124	215	6.077	1.966	1.244
	58.152	1.584	0.125	303	5.930	1.891	1.269

Conclusion

We have successfully synthesized and characterized TiO_2/silver with dye via the doctor blade technique. The structure of the cells is polycrystalline with a most outstanding peak at 2 theta angles of 30.375 ° and 30.464 ° corresponding to (200) therefore, secondary peaks were noticed at 2 theta angles of 24.891°, 27.509°, 32.915°, 27.509°, 35.296°, 38.814°, 43.152°, 47.579°, 53.231°, and 59.130° for TiO_2 and 26.116°, 27.835°, 32.667°, 36.195°, 39.802°, 41.926°, 47.173°, 52.084°, and 58.152° for $TiO_2/Ag_{0.1}$/Neem leaf, $TiO_2/Ag_{0.1}$/soursop leaf, and $TiO_2/Ag_{0.1}$/cassava leaf which corresponds to (101), (004), (105), (211), (204), (116), (220), (215), and (303) subsequently. The sensitized TiO_2/silver with dye recorded an efficiency of 0.49%, 0.03%, 0.05%, and 0.22% for *Azadirachtaindica*(neem), *Annonamuricata* (Soursop leaf), *Manihotesculenta* (cassava leaf), and Myrianthusarboreus (Coat button leaf), respectively. The optical energy bandgap was observed to be 2.32 eV for TiO_2 and 2.52 eV, 2.31 eV, 2.49 eV, and 2.51 eV for Neem, Soursop Cassava, and Giant yellow mullbery leaf dye.

Acknowledgments

The success of this study is attributed to the contributions of all the authors.

ORCID

Imosobomeh L. Ikhioya : 0000-0002-5959-4427

Reference

[1]. M.S. Ahmad, A.K. Pandey, N. Abd Rahim, *Renewable and Sustainable Energy Reviews*, **2017**, *77*, 89-108. [Crossref], [Google Scholar], [Publisher]
[2]. B. Roose, S. Pathak, U. Steiner, *Chemical Society Reviews*, **2015**, *44*, 8326-8349. [Crossref], [Google Scholar], [Publisher]
[3]. A.A. Mohammed, A.S.S. Ahmad, W.A. Azeez, *Advances in Materials Physics and Chemistry*, **2015**, *5*, 361-367. [Crossref], [Google Scholar],
[4]. K.-W. Min, S.M. Chao, M.T. Yu, C.T. Ho, P.R. Chen, T.L. Wu, *Modern Physics Letters B*, **2021**, *35*, 2141005. [Crossref], [Google Scholar], [Publisher]
[5]. S.A. Mahmoud, B.S. Mohamed, H. Killa, *Frontiers in Materials*, **2021**, *8*, 714835. [Crossref], [Google Scholar], [Publisher]
[6]. J. Liu, Y. Li, S. Arumugam, J. Tudor, S. Beeby, *Materials Today: Proceedings*, **2018**, *5*, 13846-13854. [Crossref], [Google Scholar], [Publisher]
[7]. B. Raei, A. Ghadi, A. Bozorgian, *19th Int. Congr. Chem. Process Eng.*, **2010**, *7*. [Google Scholar]
[8]. M. Ahmadlouydarab, S. Javadi, F. Adel Alijan Darab, *Advanced Journal of Chemistry, Section A*, 2023, *6*, 352-365. [Crossref], [Publisher]
[9]. A. Ahmadpour, A. Bozorgian, *Eurasian Journal of Science and Technology*, **2021**, *1*, 28-39. [Crossref], [Publisher]
[10]. A.I. Kontos, A.G. Kontos, D.S. Tsoukleris, M.-C. Bernard, N. Spyrellis, P. Falaras, *Journal of materials processing technology*, **2008**, *196*, 243-248. [Crossref], [Google Scholar], [Publisher]
[11]. K.H. Ko, Y.C. Lee, Y.J. Jung, *Journal of colloid and interface science*, **2005**, *283*, 482-487. [Crossref], [Google Scholar], [Publisher]
[12]. E.N. Josephine, O.S. Ikponmwosa, T. Alomayri, I.L. Ikhioya, *Journal of Medicinal and Nanomaterials Chemistry*, **2023**, *5*, 199-212. [Crossref], [Publisher]
[13]. J.-p. ZOU, R.-z. WANG, *Transactions of Nonferrous Metals Society of China*, **2012**, *22*, 2691-2699. [Crossref], [Google Scholar], [Publisher]
[14]. D.F. Underwood, T. Kippeny, S.J. Rosenthal, *The Journal of Physical Chemistry B*, **2001**, *105*, 436-443. [Crossref], [Google Scholar], [Publisher]
[15]. K.I. Udofia, I.L. Ikhioya, D.N. Okoli, A.J. Ekpunobi, *Journal of Medicinal and Nanomaterials Chemistry*, **2023**, *5*, 135-147. [Crossref], [Publisher]
[16]. H. Shah, S. Afzal, M. Usman, K. Shahzad, I. Ikhioya, *Advanced Journal of Chemistry, Section A*, **2023**, *6*, 342-351. [Crossref], [Google Scholar], [Publisher]
[17]. S.G. Sarwar, I.L. Ikhioya, S. Afzal, I. Ahmad, *Hybrid Advances*, **2023**, *4*, 100105. [Crossref], [Google Scholar], [Publisher]
[18]. S.O. Samuel, C.K. Ojoba, E. Ogherohwo, E.O. Ojegu, J. Zhimwang, A. Ekpekpo, I.L. Ikhioya, *Journal of the Indian Chemical Society*, **2023**, *100*, 100992. [Crossref], [Google Scholar], [Publisher]
[19]. S.O. Samuel, M.F. Lagbegha-ebi, E. Ogherohwo, I.L. Ikhioya, *Results in Optics*, **2023**, *13*, 100518. [Crossref], [Google Scholar], [Publisher]
[20]. I. Rufus, A. Peter, S.O. Aisida, I.L. Ikhioya, *Results in Optics*, **2023**, *12*, 100464. [Crossref], [Google Scholar], [Publisher]
[21]. P. Pongwan, B. Inceesungvorn, K. Wetchakun, S. Phanichphant, N. Wetchakun, *Engineering Journal*, **2012**, *16*, 143-152. [Crossref], [Google Scholar], [Publisher]
[22]. J. Jayachithra, K. Elampari, M. Meena, *IOP Publishing*, **2022**, *1263*, 012018. [Crossref], [Google Scholar], [Publisher]
[23]. O. Ikechukwu, I.L. Ikhioya, *Asian Journal of Green Chemistry*, **2024**, *8*, 137–149. [Crossref], [Publisher]
[24]. X. Hou, K. Aitola, P.D. Lund, *Energy Science & Engineering*, **2021**, *9*, 921-937. [Crossref], [Google Scholar], [Publisher]
[25]. J. Highfield, *Molecules*, **2015**, *20*, 6739-6793. [Crossref], [Google Scholar], [Publisher]
[26]. A.A. Hendi, M.M. Alanazi, W. Alharbi, T. Ali, M.A. Awad, K.M. Ortashi, H. Aldosari, F.S. Alfaifi, R. Qindeel, G. Naz, *Journal of King Saud University-Science*, **2023**, *35*, 102555. [Crossref], [Google Scholar], [Publisher]
[27]. V. González-Verjan, B. Trujillo-Navarrete, R.M. Félix-Navarro, J.D. de León, J. Romo-Herrera, J. Calva-Yáñez, J. Hernández-Lizalde, E. Reynoso-Soto, *Materials for Renewable and Sustainable Energy*, **2020**, *9*, 1-8. [Crossref], [Google Scholar], [Publisher]

[28]. M. Giannouli, *International Journal of Photoenergy*, **2013**, *2013*. [Crossref], [Google Scholar], [Publisher]
[29]. A. Fujimori, H. Nakahara, *Chemistry letters*, **2003**, *32*, 2-3. [Crossref], [Google Scholar], [Publisher]
[30]. S. Borbón, S. Lugo, D. Pourjafari, N. Pineda Aguilar, G. Oskam, I. López, *ACS omega*, **2020**, *5*, 10977-10986. [Crossref], [Google Scholar], [Publisher]
[31]. F.-Q. Bai, W. Li, H.X. Zhang, *Titanium Dioxide*, **2017**, 229-248. [Google Scholar], [Publisher]
[32]. A. Ali, S. Afzal, T. Khaleeq, H. Shah, M. Usman, and L. Imosobomeh, *Journal of Nano and Materials Science Research*, **2023**, *2*, 117–122. [Crossref], [Google Scholar], [Publisher]
[33]. Y. Akila, N. Muthukumarasamy, D. Velauthapillai, *Elsevier*, **2019**, 127-144. [Crossref], [Google Scholar], [Publisher]
[34]. I. Ahmad, J. Razzaq, A. Ammara, F. Kaleem, M. Qamar, S. Ilahi, I.L. Ikhioya, *Advanced Journal of Chemistry, Section A*, **2024**, [Crossref], [Google Scholar], [Publisher]
[35]. S. Afzal, S. Tehreem, T. Munir, S.G. Sarwar, L.I. Ikhioya, *Journal of Nano and Materials Science Research*, **2023**, *2*, 104-109. [Crossref], [Google Scholar], [Publisher]
[36]. E.J. Chukwuemeka, N.A. Osita, A.O. Odira, U. Chinwe, *Advanced Journal of Chemistry, Section A*, **2024**, 7: 27–40. [Crossref], [Google Scholar], [Publisher]
[37]. I.L. Ikhioya, N.I. Akpu, E.U. Onoh, S.O. Aisida, I. Ahmad, M. Maaza, F.I. Ezema, *Journal of Medicinal and Nanomaterials Chemistry*, **2023**, *2*, 156–167. [Crossref], [Publisher]
[38]. I.L. Ikhioya, A.C. Nkele, *Results in Optics*, **2023**, *12*, 100494. [Crossref], [Google Scholar], [Publisher]
[39]. I.L. Ikhioya, S.O. Aisida, I. Ahmad, F.I. Ezema, *Chemical Physics Impact*, **2023**, *7*, 100269. [Crossref], [Google Scholar], [Publisher]
[40]. I.L. Ikhioya, A.C. Nkele, F.U. Ochai-Ejeh, *Materials Research Innovations*, **2023**, 1-7. [Crossref], [Google Scholar], [Publisher]